Assessment of Female Human Body Models for Ballistic Impact Analysis with Post Mortem Human Subject (PMHS) Data Evaluation: A Comparative Study with Various Impact Loading Conditions

Marcin Jenerowicz, Patrick Matt, Matthias Boljen, Stefan Hiermaier

Abstract The present study analyses numerically the assessment capability of the female human body models GHBMC F05–P and VIVA+ F50 with regard to blunt trauma by a number of benchmark load cases. Three load cases from literature in regard to post-mortem human subject data, impact conditions by Bir *et al.* (2000), and three comparative impact conditions were applied. The latter, by applying impact loading with approximation of 3D surface of armour back face displacement. This load case, where no penetration occurred, contains a body armour with a hard-ballistic plate; 9 mm silicon carbide and 10 mm ultra-high molecular weight polyethylene, and a soft-ballistic component with 40–layer aramid fabric. Additionally, a load case with a non-lethal SIR 40x46 projectile impact was applied. For the evaluation of the blunt trauma, the Viscous Criterion, the Blunt Criterion and the maximum strains in the impact area were used. The evaluation was performed at two locations: mid-sternum ribs levels 3–4 and rib bone cartilage junction area at level 4. In all cases, the results show the deficits of the models and that their application is also limited to analysing blunt trauma.

Keywords Back Face Displacement (BFD), Behind Armour Blunt Trauma (BABT), Finite Element Simulation, Female Human Body Models (F-HBM), Injury Criteria.

I. INTRODUCTION

Behind armour blunt trauma (BABT) has been defined as the result of non-penetrating ballistic impact injuries caused by the rapid deformation of personal protection equipment (PPE) [1]. A definition for injuries occurring when body armour is impacted, but not perforated, has been suggested that separates injuries that include skin laceration from those that are restricted to skin contusion and rib damage [2]. During the impact event, the body armour and underlying tissues accelerate and deformation occurs. Stress waves are generated on the impact surface and propagate through the body armour and the underlying tissues [3-4]. These highly dynamic loads and resulting applied shear stresses may cause superficial contusion, soft tissue rupture, rib fracture, pulmonary contusion, and cardiac injuries depending on the impact location [5-6]. The velocity of the rear surface of the deforming armour experiences a swift increase, reaching its peak in a matter of microseconds, then undergoes a sharp decline until the maximum deflection of the back-face deformation (BFD) is achieved. This value is influenced by factors such as projectile type, velocity, and the composition of the body armour [7]. A commonly used measure in body armour standard test methods is to record the depth of the permanent indentation formed in a block of *Roma Plastilina No. 1*. The United States Department of Justice (DOJ) described a static 44 mm maximum BFD as the pass/fail threshold for ballistic armour certification, which provides a baseline metric for comparing armour effectiveness with regard to BFD [8-9]. However, the BFD does not correlate specific BABT type and severity of potential injuries in humans [10] and clay has a considerable volumetric rebound, causing the final measured deformation to be smaller than the maximum deformation [11-12]. There has been an increasing awareness of BABT as an injury mechanism in both the military and civilian environments [6][13].

Research focused on BABT experienced by female wearers of body armour appears to be limited to the studies conducted by Wilhelm and Bir [14-15]. A comparison of BABT injuries between female and male US police officers suggested a higher risk of injury among female officers [14-15]. The data were gathered from the *IACP/DuPont*

M. Jenerowicz (e–mail: marcin.jenerowicz@emi.fraunhofer.de; tel: +49–761–2714–359) is a Research Fellow at the Fraunhofer Institute for High–Speed Dynamics, Ernst–Mach–Institute (EMI), and a PhD candidate at the Faculty of Engineering of the Albert–Ludwigs–University in Freiburg, Germany. S. Hiermaier is Professor for Sustainable Systems Engineering at the Faculty of Engineering of the Albert–Ludwigs–University and the Director of the Fraunhofer Institute for High–Speed Dynamics, EMI. P. Matt and M. Boljen are affiliated with the Fraunhofer Institute for High–Speed Dynamics, EMI, Germany.

Survivor's Club, with 14 survivors (four female) consenting to participate in the study. Based on the severity of injuries sustained, an Abbreviated Injury Score (AIS) was assigned. The injuries of the four female participants were rated as AIS=3, 3, 1 and 1, respectively. In contrast, eight male participants were assigned AIS=1, one AIS=2, and one AIS=3, though the authors acknowledge the limited sample size. Higher AIS scores were associated with open wounds, lung contusions, and rib fractures.

The baseline of the following investigation is the categorisation of the BABT assessment possibility of commercially and freely available finite element (FE) female Human Body Models (HBMs) in order to create a better basis for the different characteristics and reactions of the bodies of female and male test subjects.

II. METHODS

The following section outlines the general approach of assessment, FE methods used and the adaptation of the female HBM models: Global Human Body Model Consortium (GHBMC) F05–P (v.5.3.4, detailed) representing a 5th percentile female (height 150 cm, weight 49.9 kg) and the VIVA+ F50 a 50th percentile female (height 162 cm, weight 62.3 kg), which were used for the analysis of the present study [16-17]. In addition, the principles of the injury criteria used to evaluate the results are discussed.

Evaluation Principles

For the assessment of the two female HBMs, comparative simulations were performed to common ballistic impact post-mortem human subject (PMHS) studies [12][18-19]. These test corridors are predominantly used because they are clearly documented and relatively simple to reproduce. Other sources for PMHS testing for ballistic applications refer to specific use cases for the investigation of BABT [20] or the recreation of field cases with reference to blunt trauma [7][21]. These could be used for further validation studies if the subject data can be used to retrospectively determine gender information.

For better comparability of the female HBMs to the test corridors and the specific data of the female PMHS, the original data were revised extensively. The biomechanical response to an impact depends on the physical characteristics of the individual PMHS. Therefore, a difference in the response of each specimen to a prescribed impact condition is always present. In an effort to analyse the data, Bir *et al.* used the following normalisation [18]:

$$\begin{aligned} &\text{Normalised displacement} = \text{displacement t} \times \lambda \\ &\text{Normalised force} = \text{force} \times \lambda^2 \\ &\text{Normalised acceleration} = \text{acceleration} \times \lambda^{-1} \\ &\text{Normalised time} = \text{time} \times \lambda \end{aligned} \tag{1}$$

where the basic scaling factor λ is defined as chest depth of 50th percentile male / specimen chest depth. The chest depth for the 50th percentile male was considered to be 236 mm [22]. In order to be able to use the data from the female PMHS for comparison with female HBMs, these were denormalised. The specific chest depth and thus the corresponding λ is known ([12], Table 3.1). Thus, the original measurement data were restored. The following Table I shows the anthropometric data for the female PMHS tested by Bir *et al.* [12]:

TABLE I
ANTHROPOMETRIC DATA FOR FEMALE CADAVERIC SPECIMENS TESTED AND IMPACT CONDITIONS FOR SPECIFIED TESTS (*FROM WAYNE STATE UNIVERSITY, OTHERS FROM THE UNIVERSITY OF MICHIGAN) [12]

Test #	Specimen #	Age (years)	Mass (kg)	Stature (cm)	Impactor A	Impactor B	Impactor C
NIJ 4	599*	68	75	165		X	
NIJ 6	29422	76	75	171			X
NIJ 9	29676	76	71	158			X
NIJ 10	29610	70	79	168	X	X	X
NIJ 12	864*	76	72	168	X		X

To ensure comparability with the female HBMs, only the original female PMHS data (subject ID description, see Table I) were used. For this purpose, a new normalisation scaling factor κ was introduced, which is defined as follows: κ = chest depth of 50th percentile female / specimen chest depth. The chest depth for the 50th percentile

female was adapted from the VIVA+ F50 model and equals 227 mm. κ was used for the new normalisation as λ according to Equations (1). The deviation from the original data was up to 11% and was therefore corrected. The new PMHS characteristic values of IC–A, IC–B and IC–C were averaged and included in Figures 3 and 4 (Avg. Female). For the displacement-time curve of IC–B, only the data of NIJ 10 exists, therefore only these are shown in the results and the resulting force-displacement diagram.

Computational Modelling

The impactors and impact conditions (IC) according to [12] have been adopted and implemented in LS-DYNA; IC–A: 140 g at 20 m/s; IC–B: 140 g at 40 m/s; and IC–C: 30 g at 60 m/s. (Impactor A/B/C: rigid, solid, A/B: 176900 elements, C: 49532 elements.) Impact location was aligned with the centre of the T8 vertebrae according to [12].

LS-DYNA calculates the solution by running over all the nodes in the model at each time step. It analyses the total force on each node from the previous time step, uses that to find the acceleration of that node, and then finds the displacement of that node. The node is then moved by the particular offset. The calculation then updates the strain on the connecting element. These are used to evaluate the material constitutive equations to get the stresses, which are added to the forces acting on the neighbouring nodes in the next time step. This series of calculations, behaving like a wave, propagates through the mesh. The decisive aspect is to set the time increment such that the code can calculate the displacements of the next node before the wave from the previous node calculation can reach it. With very high dynamic loads, the setting of the time increments and the definition of the control parameters are important to ensure the stability of the simulation. For this reason, the control properties of the two HBMs were adapted, and those of the GHBMC model were adopted for the VIVA+ model. This includes the adjustment of the time step size for mass-scaled solutions (dt2ms) to -1.67E-4 ms (previously -0.33E-3 ms). In addition, damping factors are implemented in the material properties, which are required to remove high-frequency oscillations. For the GHBMC F05 in part “SK-Thorax_3D”, material: simplified quasi-hyper-elastic rubber model (*Adipose_37percent_srate*), damping 10%; and for the VIVA+ F50 in part “Soft-Skin”, material: layered orthotropic composite model (*HE-Skin_Manschot_et_al_1986*), damping 5%. These default settings at the material level were not changed in order to retain the original properties.

In addition to the previously mentioned impact boundary conditions according to Bir *et al.* [12], three further benchmark impact conditions were simulated, which are explained in more detail subsequently. For the additional impact boundary condition, in an earlier research [23], the same use case as in the present study was applied for the male 50th percentile (M50) GHBMC: the ballistic impact of a 7.62 mm × 51 AP8 projectile on a hard-ballistic plate made of 9 mm silicon carbide (SiC) and 10 mm of an ultra-high-molecular-weight polyethylene (UHMW–PE) component, in which no penetration of the hard-ballistic plate occurred [23]. Figure 1 (a) shows the hard-ballistic plate (9 mm SiC, 10 mm UHMW–PE) after an impact with the AP8 projectile at $v_P = 913$ m/s, with the remaining BFD seen in Figure 1 (a). Figure 1 (b) shows the corresponding simulation of the performed experiment.

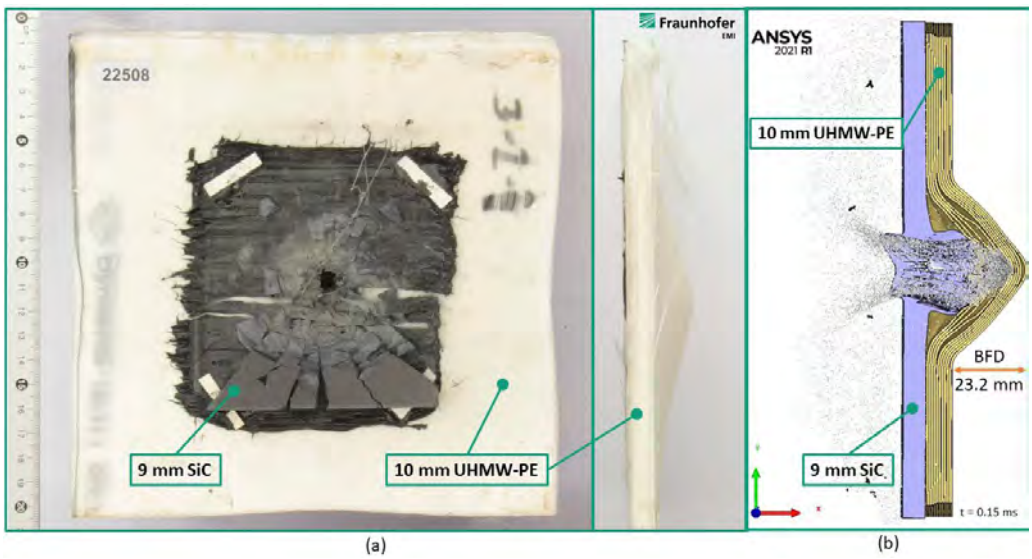

Fig. 1. (a) Hard-ballistic plate of 9 mm silicon carbide (SiC) and 10 mm of an ultra-high-molecular-weight polyethylene (UHMW–PE) after impact with 7.62 mm x 51 AP8–Projectile at $v_P = 913$ m/s). (b) Corresponding simulation of the

performed experiment with Ansys Autodyn, maximum back face deformation (BFD) 23.2 mm at 0.15 ms [23].

Jenerowicz *et al.* presented a new methodology in which the time-displacement boundary conditions of the last layer of the UHMW–PE are transferred to a separate Substitute Impact Layer (SIL) for the approximation of the 3D surface of the BFD [23]. A modelling procedure has been developed to convert plain fabric sheets from a 2D form to a 3D shape conforming to the body surface of the individual wearing the fabric [24]. Employing a dynamically evolving stamp geometry to continually revert the flattened body surface back to its original form, the method mirrors the process of deep drawing. This technique offers a straightforward means of draping flexible objects over various contours [25]. The soft ballistics packages in this study were modelled using this method. The soft ballistics consist of three fabric packages containing 13, 14 and 13 individual plies, respectively. The plies are oriented alternately in the 0°/90° and ±45° orientations, with each ply having a thickness of 0.28 mm [25]. For the forming algorithm, only the innermost layer of the entire vest was subjected and, after forming, subsequently stacked to the actual number of layers. Following draping, the individual plies were packed via boundary conditions to form the stitched package of 38 layers [25]. The virtual stamps were generated by an upscaled duplicate of the GHBMC F05 and the VIVA+ F50 body surfaces.

The SIL was applied at two specific areas for the present study. Point of interest (POI) 1 is located directly over the midline of the sternum, mid between 3rd–4th ribs and POI–2 at the sternal end of the 4th rib at the junction between cortical bone and the costal cartilage. Figure 2 shows the applied SIL deformation on the GHBMC F05 and VIVA+: Fig. 2 (a) and (c) at POI–1 and Fig. 2 (b) and (d) at POI–2, all at t = 0.30 ms.

(a) (b) (c) (d)

Fig. 2. Soft-ballistic armour deformation by substitute impact layer (SIL) on the GHBMC F05–P at t = 0.30 ms: (a) impact location POI–1; (b) impact location POI–2, (SIL) on the VIVA+ F50 at t = 0.30 ms; (c) impact location POI–1; (d) impact location POI–2.

In addition, a non-lethal projectile *B&T SIR GL–06* of caliber 40x46 mm was modelled in order to investigate the influence of a further non-penetrating impact load on the body. The SIR 40x46 projectile consists of a linear viscoelastic model, solid, 1116 elements. The simulations were performed with an impact velocity of 75 m/s (exit velocity 85 m/s) [26] at the same impact location as POI–1. This was selected as a real impact scenario that is comparable to IC–C.

Injury Criteria

The assessment of blunt trauma is based on research conducted by Clare *et al.* in the 1970s [27], which has evolved into a multi-parameter model [28]. The Blunt Criterion (BC) is defined by Equation (2):

$$\mathrm{BC} = \ln\left(\frac{\mathrm{E_{kin}}}{\mathrm{t_{BWT}} \cdot \mathrm{d_P} \cdot \mathrm{W}^{1/3}}\right)$$
$$\text{with } \mathrm{E_{kin}} = \frac{1}{2} \cdot \mathrm{m_1} \cdot {\mathrm{v_1}}^2 \text{ and } \mathrm{t_{BWT}} = \mathrm{k} \cdot \mathrm{W}^{1/3} \quad (2)$$

where $\mathrm{E_{kin}}$ is the kinetic energy of the projectile at impact in [J], with $\mathrm{m_1}$ as the mass of the projectile in [kg], $\mathrm{v_1}$ as the velocity of the projectile in [m/s], $\mathrm{t_{BWT}}$ is the body wall thickness (BWT) of the individual in [cm], *k* is 0.711 for male and 0.593 for female subjects, $\mathrm{d_P}$ is the diameter of the projectile in [cm], and *W* is the mass of the

individual (or struck target) in [kg]. Since the transfer of impulse energy to the rest of the body is relatively slow in relation to the rate of injury on impact, the body mass affected is only the effective mass of the part of the torso that moves with the projectile on impact. Nevertheless, the total mass of the individual is used. This is due to the relatively minor influence of this variable in the overall calculation and the fact that it can only be estimated in the PMHS test, which would introduce additional uncertainties. The momentum of the projectile was obtained by the momentum of the combined mass of the body part or armour and the projectile after impact, in Eq. (2) [28]. Real thickness data from human subjects to calculate the parameter *k* was taken on the lateral rib cage directly over the ribs and the centre of the lung [28]. For the GHBMC F05 with a total mass of 49.93 kg, the BWT is t_{BWT} = 2.18 cm and for the VIVA+ F50 with *W* = 62.30 kg, t_{BWT} = 2.35 cm.

The second injury criterion under consideration is the Viscous Criterion (VC) [29], extensively validated for motor-vehicle occupants and only certain relevant injury cases involving ballistic impacts on PMHS [19]. The VC assesses the injury tolerance of soft tissue during the rapid phase of body deformation upon impact, known as the viscous response. It is expressed by the following equation:

$$\mathrm{VC} = \mathrm{V(t)} \cdot \mathrm{C(t)} = \frac{d\mathrm{D(t)}}{d\mathrm{t}} \cdot \frac{\mathrm{D(t)}}{\mathrm{D_0}} \tag{3}$$

where D(t) is the chest deflection and D_0 the initial chest depth (GHBMC F05–P: D_0 = 214 mm, VIVA+ F50: D_0 = 227 mm). Analysis conducted by Viano and Lau suggests that the combined effect of velocity and compression ($V(t)\cdot C(t)$) offers better predictive capability for injury compared to either velocity or compression alone [29]. Furthermore, they validated the VC by analysing available data from PMHS, indicating a strong correlation between the maximum viscous response and the risk of severe soft tissue and internal organ injuries. In a study by Bir and Viano [19], different conditions of blunt ballistic impacts (IC–A, IC–B and IC–C) produced distinct injury responses, differing from those observed in automotive literature for lower speed impacts [18]. This underscores the need for further validation of the VC in predicting injuries from blunt ballistic impacts, with a cautious approach advised when comparing collected simulation data.

In the present study, the displacement-time data at the examined locations POI–1 and POI–2 was used to calculate the biomechanical parameter $\mathrm{VC_{max}}$. The calculation on both female HBMs for POI–1 was done using the displacement-time data and the corresponding velocity for the centre of mass of the sternum. For POI–2, six nodes were selected from the sternal end on the anterior side centrally along the length of the costal arch and also analysed for displacement-time data and corresponding velocities. The position and quantity of selected nodes represent an averaged value utilised for the analysis. The maximum displacement identified exhibits significant variation relative to the distance from the sternal end. This value can vary considerably depending on the arrangement and quantity of nodes. Further investigation into the impact of these parameters on the VC and potentially mesh size is subject of future studies.

The study conducted by Forman *et al.* [30] outlines a technique for refining stochastic strain-based thoracic injury risk functions (IRF) tailored to specific HBM (THUMS v.4.1 and GHBMC v.6.0). These local strain-based IRFs were adjusted to achieve the closest alignment with injury outcomes observed in tests with PMHS. Findings revealed that directly applying rib cortical bone ultimate strain data to the HBM could lead to an underestimation of rib fracture risk compared to PMHS test references. However, optimising the local strain IRF for each model tended to yield more accurate injury risk predictions, aligning well with PMHS tests and field data-derived risks. By fine-tuning the local strain IRF for a specific HBM, this framework offers a method to achieve consistent injury risk predictions across HBMs with varying constructions [30]. Based on this study, the probabilities of a possible rib failure were calculated. It should be noted that there are no valid risk curves for female PMHS and HBM, therefore the curves for the GHBMC M50 were used. In addition, the maximum strains stated contradict the strains actually determined in single rib tests carried out by Agnew *et al.* [31]. These suggest a maximum strain at break of approximately 1.5% for young adults (21–40 years) and approximately 1.25% for middle-aged adults (41–60 years). Both studies [30-31] invariably refer to load cases from the automotive sector, which should therefore be viewed with caution when comparing the results of BABT comparative studies conducted at significantly higher strain rates.

For all defined load cases the kinetic energies were calculated from Eq. (2), with the corresponding masses of the impactors and the soft-ballistic package, by assuming that the debris of projectile and ceramic plate, weighing

41 g, would hit the soft armour with a remaining mean velocity of v = 113.4 m/s [23].

III. RESULTS

The following figures show the comparative curves of the results. Figure 3 shows the force-time and the deflection-time curves for IC–A, IC–B and IC–C with the reprocessed female PMHS data, and the general boundary conditions according to [18] compared to the simulation data of the GHBMC F05 and VIVA+ F50 models.

The force data of the simulations was determined at the contact surface between the impactor and the HBM. Due to the relatively coarse mesh size of the target surface at the HBMs, the determined data is subject to strong oscillations. For a better overview, the data curves were formed from a 9th order polynomial fit and mapped with the corresponding residuals. The partially large residuals result from the large discrepancy to the mean values of the fitted curve. The associated R^2 (adj.) values of the force-time curves are shown in Table II.

TABLE II
UNIVARIATE RESULTS FOR FORCE VALUES, R^2 (ADJ.) FOR THE 9TH ORDER POLYNOMIAL FIT IN FIGURE 3

Impact Condition	GHBMC F05	VIVA+ F50
IC–A	0.90	0.66
IC–B	0.84	0.58
IC–C	0.68	0.46

The decreasing R^2 (adj.) value with increasing velocity of the impactor shows the resulting discrepancy and reduced regression. The coarser mesh of the VIVA+ F50 model shows clear differences in the performance values. None of the curves match the comparative values. The mean reaction forces are too small for IC–A and IC–B and too large for IC–C, with the individual residuals indicating even greater deviations.

The deflection data curves are shown with the averaged characteristic values of the nodes on the HBM contact surface (n=6 in the centre of the impact location) with the standard deviation (IC–B with only available deflection data from subject NIJ 10). It should be noted that the determination of the average values over the 6 nodes influences the accuracy due to the different mesh size on the surface of the two HBMs. The resulting standard deviation is therefore larger for the VIVA+ F50 than for the GHBMC F05. The comparison of the trends shows for IC–A: both models fit the mean female PMHS data up to t = 1.0 ms, but are then above the upper limit, IC–B: both models fit the comparative value of the NIJ10 relatively well, IC–C: the GHBMC F05 fits within the specified corridor, the VIVA+ F50 is initially within the limit range up to t = 0.6 ms, but then exceeds it by over 20%.

Figure 4 shows the combined force–deflection results from Figure 3 with the conditions described above. It is clearly apparent that the specific curves do not fit the specified corridors. This will be due to the poor force-time curves with the relatively large residuals, as the displacement–time profiles fit the corridors in Figure 3 relatively well for some conditions.

Figure 5 present the maximum strains determined in the thoraxes. It shows the GHBMC F05 and the VIVA+ F50 thorax with maximum principal strains for IC–A, IC–B and IC–C according to [18], impact with SIR 40x46 projectile at 75 m/s and points of interest (POI–1: midline of the sternum, mid between 3rd and 4th ribs; POI–2: sternal end of the 4th rib at the junction between cortical bone and the costal cartilage) with substitute impact layer (SIL) back face signature according to [23] at corresponding time of maximum deflection. It can be clearly seen that the maximum strains in the costal cartilage are exceeded for all load cases. Due to the relatively large local displacements of the sternum, the surrounding soft tissue is heavily stressed.

The characteristic values from all subjects and results were combined with the injury data and AIS rankings from literature [19] and are summarised in Table III. The negative BC for low impact energies results from the logarithmic Equation (2). It should be noted that the correlation of the value to the AIS scores has a low threshold, above which an AIS of 2–3 was defined [19]. Accordingly, except for IC–A, all conducted analyses are rated AIS 2–3 or higher, which in turn does not correspond to the female PMHS autopsy report from [12].

Table IV shows the determined maximum principal strains in the ribs 3, 4 and 5 on the left and right side and the probability of failure (calculated from the maximum values in the respective boundary conditions) according to Forman *et al.* [30]. The determined probability does not consider the failure of the costal cartilage. Therefore, compared to Figure 5, only the ribs in the impact scenario SIL POI–2 are affected for both HBMs.

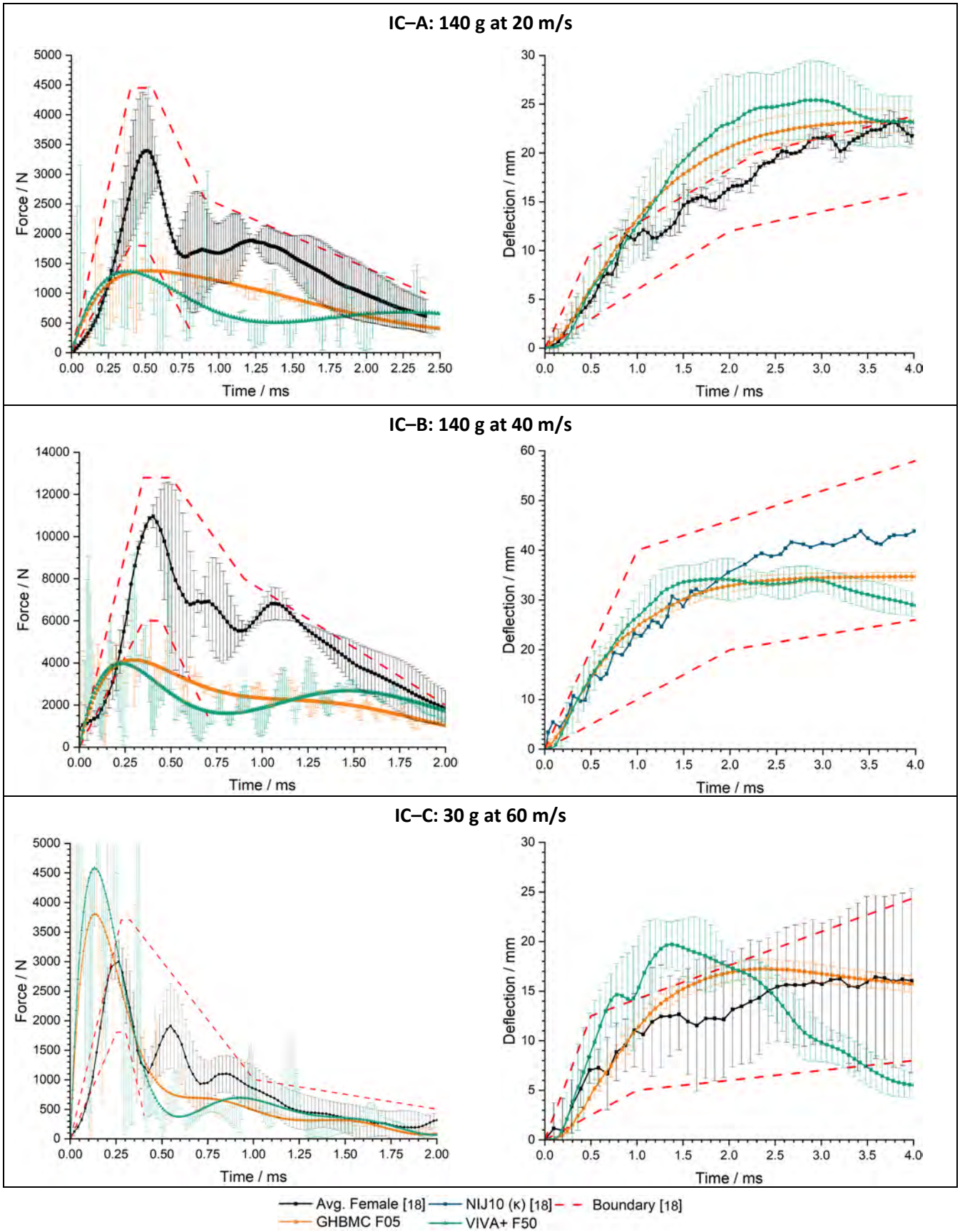

Fig. 3. Force-time and deflection-time curves for impact conditions (IC)–A, B and C with averaged female PMHS data (IC–B with only available deflection data from subject NIJ 10), and the general boundary conditions according to [18]

compared to the simulation data of the GHBMC F05 and VIVA+ F50 models; data curves are shown using 9th order nonlinear curve fit; force data obtained from the contact surface between the impactor and the HBM with the associated residuals; deflection data obtained from the averaged characteristic values of the nodes on the HBM contact surface (n=6 in the centre of the impact location) with the standard deviation.

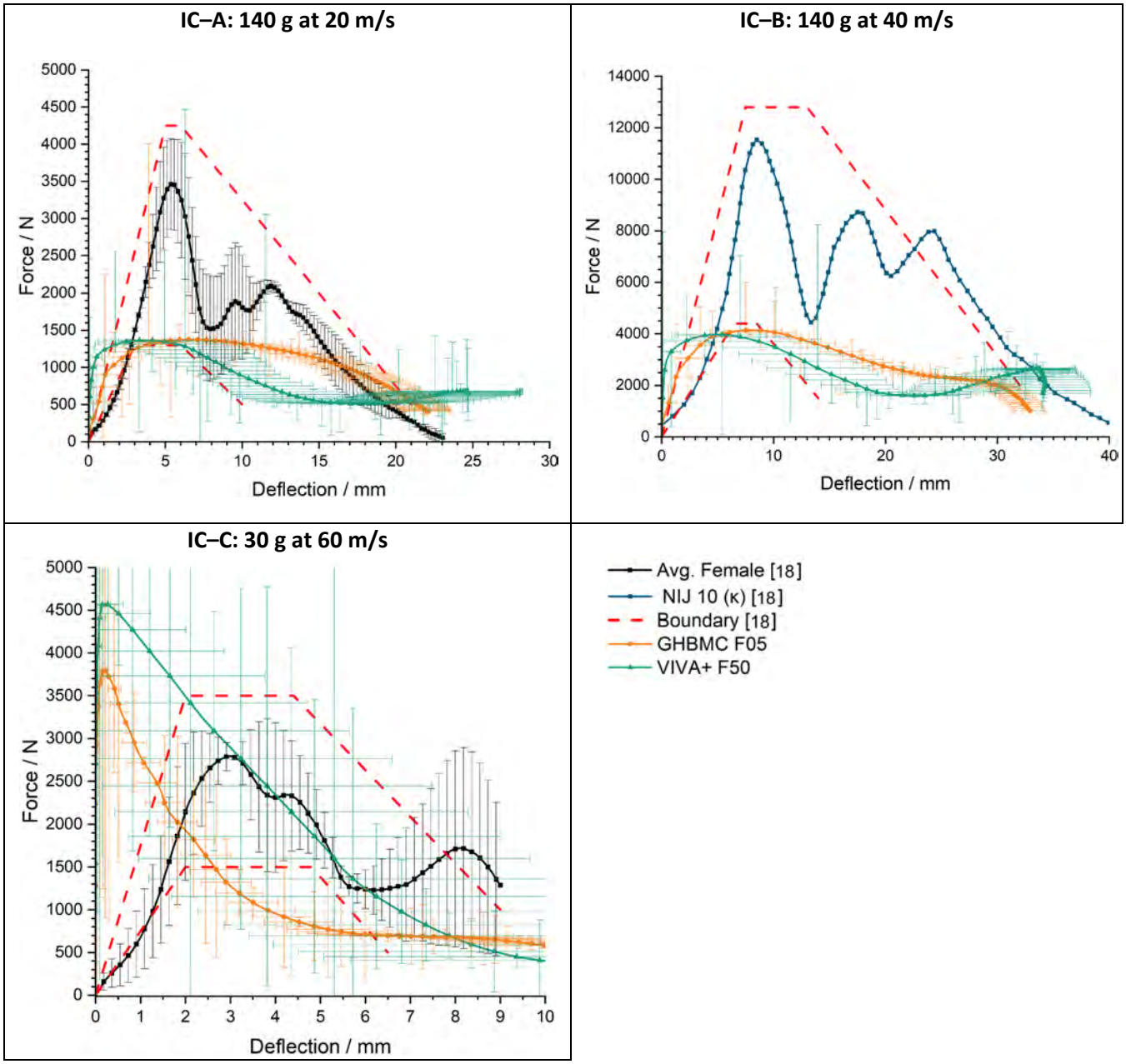

Fig. 4. Force-deflection curves for impact conditions (IC)–A, B and C with averaged female PMHS data (IC–B with only available data from subject NIJ 10), and the general boundary conditions according to [18] compared to the simulation data of the GHBMC F05 and VIVA+ F50 models; data curves are shown using 9th order nonlinear curve fit with the associated residuals obtained from the contact surface between the impactor and the HBM for the force and the averaged characteristic values of the nodes on the HBM contact surface (n=6 in the centre of the impact location) with the standard deviation for the deflection.

GHBMC F05

IC–A	IC–B	IC–C
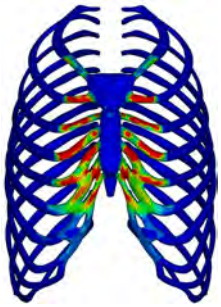	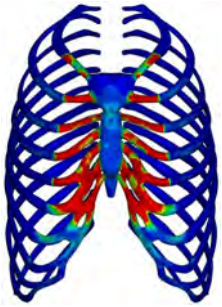	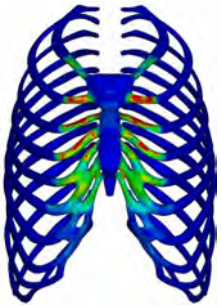
t = 3.50 ms	t = 3.50 ms	t = 2.35 ms

VIVA+ F50

IC–A	IC–B	IC–C
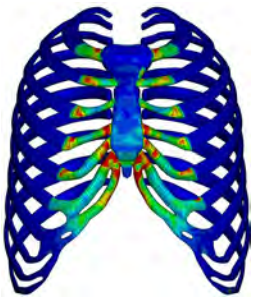	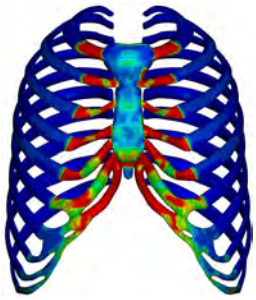	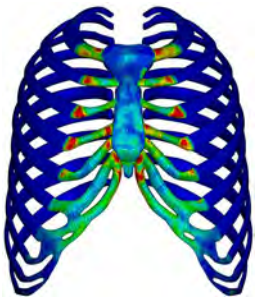
t = 3.50 ms	t = 3.50 ms	t = 2.35 ms

GHBMC F05

SIR 40x46	POI–1	POI–2
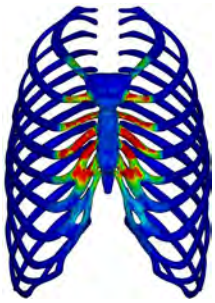	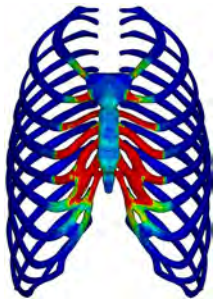	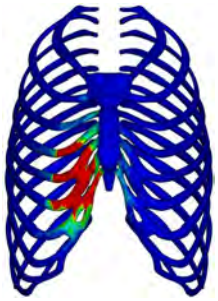
t = 1.30 ms	t = 0.60 ms	t = 0.3 ms

VIVA+ F50

SIR 40x46	POI–1	POI–2
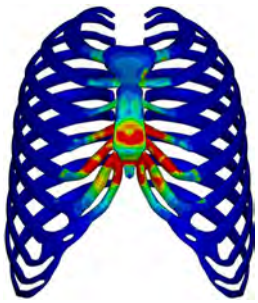	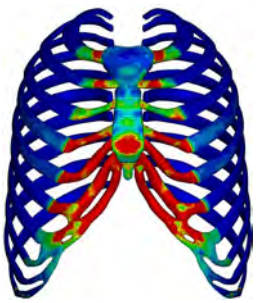	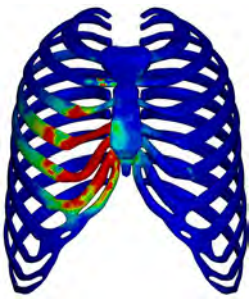

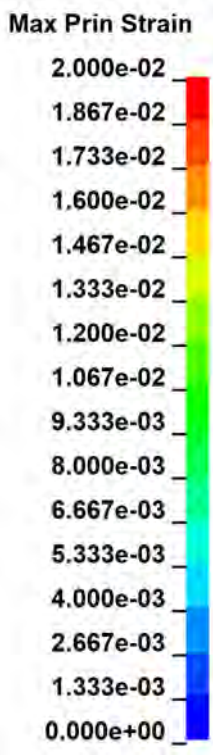

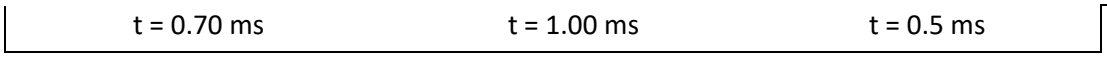

Fig. 5. GHBMC F05 and VIVA+ F50 thorax maximum principal strains for impact conditions (IC)–A, B and C according to [18], impact with SIR 40x46 projectile at 75 m/s and points of interest (POI–1: midline of the sternum, mid between 3rd and 4th ribs; POI–2: sternal end of the 4th rib at the junction between cortical bone and the costal cartilage) substitute impact layer (SIL) back face signature according to [23] at corresponding time of maximum deflection.

TABLE III
CHARACTERISTIC VALUES AND RESULTS OVERVIEW WITH ASSOCIATED PMHS COMPARATIVE DATA ACCORDING TO BIR *ET AL.* [18-19]

HBM / Subject	Impact Condition	Mass (kg)	Velocity (m/s)	Energy (J)	Diameter (cm)	Weight (kg)	BWT (cm)	BC (–)	VC_{max} (m/s)	AIS
GHBMC F05	IC–A	0.14	20	28.0	3.7	49.93	2.18	-0.06	0.94	0
	IC–B	0.14	40	112.0	3.7	49.93	2.18	1.33	3.20	2–3
	IC–C	0.03	60	54.0	3.7	49.93	2.18	0.60	1.44	2–3
	SIL POI–1	0.041	113.4	263.62	7.0	49.93	2.18	1.55	8.22	3+
	SIL POI–2	0.041	113.4	263.62	7.0	49.93	2.18	1.55	10.39	3+
	SIR 40x46	0.032	75	90.0	4.0	49.93	2.18	1.03	2.83	2–3
VIVA+ F50	IC–A	0.14	20	28.0	3.7	62.30	2.35	-0.21	2.21	0
	IC–B	0.14	40	112.0	3.7	62.30	2.35	1.18	4.99	2–3
	IC–C	0.03	60	54.0	3.7	62.30	2.35	0.45	8.07	3+
	SIL POI–1	0.041	113.4	263.62	7.0	62.30	2.35	1.40	8.77	3+
	SIL POI–2	0.041	113.4	263.62	7.0	62.30	2.35	1.40	9.64	3+
	SIR 40x46	0.032	75	90.0	4.0	62.30	2.35	0.88	10.69	3+
NIJ 10	IC–A	0.14	16.80	19.76	3.7	79	2.54	-0.71	0.51	0
NIJ 12	IC–A	0.14	22.19	34.47	3.7	72	2.47	-0.10	0.46	0
NIJ 4	IC–B	0.14	43.24	130.88	3.7	79	2.54	1.18	2.18	2
NIJ 9	IC–C	0.03	62.85	59.25	3.7	71	2.45	0.46	0.14	0
NIJ 10	IC–C	0.03	63.48	60.45	3.7	79	2.54	0.40	0.59	0
NIJ 12	IC–C	0.03	63.01	59.29	3.7	72	2.47	0.45	0.60	2

TABLE IV
DETERMINED MAXIMUM PRINCIPAL STRAINS IN RIBS AND PROBABILITY OF FAILURE FOR THE MAXIMUM VALUE IN THE RESPECTIVE BOUNDARY CONDITION ACCORDING TO FORMAN *ET AL.* [30]

HBM	Impact Condition	Maximum Principal Strains in Rib Cortical Bone (%)						Probability of Fracture [30] (%)
		Rib 3		Rib 4		Rib 5		
		R	L	R	L	R	L	
GHBMC F05	IC–A	0.44	0.49	0.32	0.32	0.15	0.18	< 0.12
	IC–B	1.04	1.29	0.79	0.72	0.36	0.45	< 4.70
	IC–C	0.30	0.37	0.24	0.23	0.14	0.15	< 0.07
	SIL POI–1	0.82	1.07	0.95	1.19	0.64	0.69	< 3.63
	SIL POI–2	1.61	0.12	3.36	0.14	2.45	0.12	< 69.66
	SIR 40x46	0.41	0.49	0.32	0.30	0.19	0.23	< 0.19
VIVA+ F50	IC–A	0.21	0.20	0.16	0.16	0.14	0.14	< 0.01
	IC–B	0.38	0.39	0.56	0.55	0.32	0.32	< 0.28
	IC–C	0.14	0.16	0.14	0.13	0.14	0.14	< 0.01
	SIL POI–1	0.36	0.35	0.40	0.45	0.45	0.57	< 0.31
	SIL POI–2	2.11	0.25	4.39	0.16	3.21	0.19	< 94.63
	SIR 40x46	0.21	0.22	0.18	0.17	0.20	0.21	< 0.01

IV. DISCUSSION

The results of the present study indicate that the models presented are currently unsuitable for ballistic investigations. The force-time curves shown in Figure 3 do not match the test corridors according to Bir *et al.* [18]. In IC–A and IC–B these curves are far too gradual, and in IC–C the initial maximum force is far too high. In addition, the scatter of the characteristic values is relatively high, as can be seen from the distribution of the residuals. These show the large difference between the observed values. This can be attributed to the analysed contact between the HBM surface and the impact bodies. Due to the relatively coarse mesh size of the target surface on the HBMs, the data obtained is subject to strong oscillations. This is due to the fact that the field of application of the HBM is primarily designed for load cases from the automotive sector, therefore no fine resolution is required in the thorax or on the surface. The fitted curve determined from the results again shows the wide discrepancy. An adjustment of the mesh resolution is essential for further investigations. The directly affected areas and parts (skin and underlying soft tissue) must be adapted to the impactor.

In contrast, the displacement-time curves are better adapted to the specified boundary conditions. As already described, these were determined using an average value that was generated over a certain number of nodes in the centre of the contact point. This also leads to observed differences between the two HBMs. The GHBMC F05 has a much finer resolution in the thorax area, which is shown by the lower standard deviation of the characteristic values determined. The VIVA+ F50 also has higher displacements in all impact conditions than the GHBMC F05. The determined maximum displacement shows a considerable fluctuation in relation to the distance from the end of the sternum. This value can vary considerably depending on the arrangement and number of nodes. Further investigation of the effects of these parameters on VC and possibly mesh size is addressed in future studies. Other reasons for these results could be the different materials used (GHBMC F05; thorax 2D: Ogden rubber model, 3D: simplified quasi-hyper-elastic rubber model, VIVA+ F50; soft skin: layered orthotropic composite material model, soft tissues: Ogden rubber model) and the defined properties. For the GHBMC F05 in part “SK-Thorax_3D”, the damping is set by default to 10% and for the VIVA+ F50 in part “Soft-Skin”, damping is at 5%. Further, the shear modulus in the GHBMC thorax soft tissue is higher, which means that the material is stiffer and deforms less when shear forces are applied.

Additionally, the control settings of the GHBMC F05 were transferred to those of the VIVA+ F50 model for stability reasons when performing the analyses. This includes changing the time step size for mass-scaled solutions (dt2ms). Mass scaling is a technique in which non-physical mass is added to a structure to achieve a larger explicit time step (artificially enlarge the time step as long as inertia effects due to the higher masses do not influence the problem solution). In this case, this may involve adding mass to a few small elements in a non-critical region where the velocity is low, and the kinetic energy is very small relative to the peak internal energy. The effects of mass scaling should nevertheless be investigated in further studies.

The strain distributions presented in Figure 5 show significantly increased characteristic values above 2% for all impact conditions, which is an indicator of final failure [31]. It should be noted that the highest strains occur predominantly in the cartilage tissue. The comparative values of Table III and the displacements shown in Figure 3 indicate the cause. IC–B has the highest energy input in direct comparison to the other impact conditions (except SIL POI–1 and POI–2), which also leads to the largest strain patterns. The PMHS comparison test with NIJ 4 has a similar energy input and leads to a classification of AIS 2, from which it can be concluded that IC–B is relatively likely to lead to an injury. The displacement-time curves also matched relatively well here. The high strain distribution of the other impact conditions (IC–A, IC–C and SIR 40x46) results from the excessive displacements. For IC–A, red areas with more than 2 % strain can be seen in both models, which would lead to at least AIS 2. The AIS values determined using the injury criteria in Table III according to Bir *et al.* [19] therefore do not correspond to the maximum strains in Figure 5. The models overestimate the effects of the impactors. This can be observed even more strongly for the two SIL conditions. For POI–1, the maximum strain ranges are even more distinctive than for IC–B and this for both HBMs. For POI–2, the impact centre is located in the transition area between the sternal end of the 4th rib and the cartilage tissue, which leads to a definitive failure of the surrounding tissue in

both models, whereby the GHBMC F05 shows higher strains. The F05 model represents a smaller physiology, which can lead to larger areas of damage with the same deformation and energy input.

It is known from previous work that the BC and VC are only suitable for evaluation to a limited extent, as the calibration to BABT is not sufficient [23]. In [19], the correlation between BC and VC was established using a few PMHS tests. Due to the limited number of tests, the threshold value that leads to a definition of AIS 2 or higher is marginal. The BC and VC values determined in the present study all lead to a rating of AIS 2+ (except for IC–A), which would also be consistent with the strains determined in the costal cartilage. However, as already described, the relative displacements and resulting strains are too large. For the selected PMHS parameters in Table III, only two cases are rated AIS 2, the rest are rated AIS 0, which would confirm the excessive values.

The calculated probabilities for rib fractures in Table IV must also be regarded as relatively insufficient. In all impact conditions, apart from POI–2, the cartilage tissue is subjected to the largest strains. Therefore, only small strains occur in the ribs. In POI–2, the 4th right rib is directly exposed, which leads to the high strains (GHBMC F05: 1.61% and VIVA+ F50: 2.11%). According to Forman *et al*. [30], the probabilities of rib failure are <69.99% and <94.63%. According to Agnew *et al*. [31], the maximum characteristic values for rib fractures are exceeded. They suggest a maximum strain at break of approximately 1.5% for young adults (21–40 years) and approximately 1.25% for middle-aged adults (41–60 years). The evaluation here was based on the GHBMC M50, due to the lack of female PMHS data, which most likely influenced the results. This again shows the under-representation of female individuals in many studies and load scenarios.

V. CONCLUSION

The current study conducts numerical analysis to assess the capabilities of the female HBMs GHBMC F05–P and VIVA+ F50 regarding blunt trauma. This assessment involves subjecting the models to impact loading conditions from PMHS tests [12][18-19]. In addition, an impact scenario was analysed while approximating the 3D displacement of an armour BFD. A specific load case from a previous study was chosen, wherein no penetration of the hard-ballistic plate occurred [23]. From this study, two impact points were selected: one at the midline of the sternum between the 3rd and 4th ribs (POI–1), where significant thorax deformations were anticipated, and another at the transition area of the 4th rib from the sternal end to the costal cartilage (POI–2), where rib loading was expected to be highest. Additionally, a load case involving impact by a non-lethal SIR 40x46 projectile at 75 m/s was applied [26], which offers a realistic comparison to IC–C. In further studies, the effect of this real impactor will be extended to other parts and impact zones.

The evaluation of blunt trauma included the use of the Viscous Criterion, Blunt Criterion, and maximum strains in the impact area. In all impact conditions performed, an AIS 2 or higher was achieved, which is not consistent with all PMHS tests. Nevertheless, it is important to take a critical look at the characteristic values determined. Certain limit values, initially defined in the HBMs for automotive applications, were utilised for these load cases. However, due to the highly dynamic and extensive loads concentrated on a significantly smaller impact area resulting from the projectile's effective range, the numerical model approaches its representational limits.

Further studies on blunt trauma using the HBMs presented require a revision of the models for the existing loading cases and a new validation by comparison with PMHS tests, considering the different characteristics of female and male PMHS. The main conclusion of the study indicates that, while the models are not yet suitable for use under the specified impact conditions and for applications related to BABT, they hold potential for future applicability in these areas if the current deficiencies are addressed.

VI. ACKNOWLEDGEMENTS

We would like to express our appreciation to the Federal Office of Bundeswehr Equipment, Information Technology and in-Service Support (BAAINBw, Koblenz, Germany), to the Bundeswehr Technical Center for Weapons and Ammunition (WTD–91 GF–450, Meppen, Germany) and to the Bundeswehr Defense Technology Center for Protection and Special Technology (WTD–52 GF–320, Oberjettenberg, Germany) for funding this work.

VII. REFERENCES

[1] Prather, R. N.; Swann, C. L.; Hawkins, C. E. (1977) Back-face Signatures of Soft Body Armors and the Associated Trauma Effects. *The Defense Technical Information Center (DTIC)*, Aberdeen, USA.

[2] Wilhelm, M.; Bir, C. (2008) Injuries to law enforcement officers: The back-face signature injury. *Forensic Science International*, **174**(1): pp. 6–11.

[3] Proud, W. G.; Goldrein, H. T.; Esmail, S. (2009) Review of wound ballistics literature: The human body and injury processes. *Proceedings of Light-Weight Armour for Defence & Security (LWAG)*, 18–19 May, 2009, Aveiro, Portugal.

[4] van Bree, J.; van der Heiden, N. (1998) Behind armour blunt trauma analysis of compression waves. *Proceedings of Personal Armour Systems (PASS98)*, 1998, Colchester, UK.

[5] Lidén, E.; Berlin, R.; Janzon, B.; Schantz, B.; Seeman, T. (1988) Some observations relating to behind-body armour blunt trauma effects caused by ballistic impact. *The Journal of Trauma*, **28**(1) Suppl: pp. 145-148.

[6] Cannon, L. (2001) Behind armour blunt trauma – An emerging problem. *Journal of the Royal Army Medical Corps*, **147**(1): pp. 87–96.

[7] Cronin, D. S.; Bustamante, M. C., et al. (2021) Assessment of Thorax Finite Element Model Response for Behind Armor Blunt Trauma Impact Loading Using an Epidemiological Database. *Journal of Biomechanical Engineering*, **143**(3).

[8] Ballistic Resistant Protective Materials - NIJ Standard 0108.01 (1985), https://nij.ojp.gov/library/publications/ballistic-resistant-protective-materials-nij-standard-010801. [21.03.2023].

[9] Ballistic Resistance of Body Armor - NIJ Standard-0101.06 (2008), https://nij.ojp.gov/library/publications/ballistic-resistance-body-armor-nij-standard-010106. [21.03.2023].

[10] Hanlon, E.; Gillich, P. (2012) Origin of the 44-mm behind-armor blunt trauma standard. *Military Medicine*, **177**(3): pp. 333–339.

[11] Op 't Eynde, J.; Pang, D. Y., et al. (2023) The Fundamental Limitations of Clay for Assessing Human Response for Behind Armour Blunt Trauma. *The 16th International Personal Armour Systems Symposium (PASS)*, 11-15 September, 2023, Dresden, Germany.

[12] Bir, C. (2000) The evaluation of blunt ballistic impacts of the thorax. Wayne State University Dissertations, May 2000.

[13] Carroll, A. W.; Soderstrom, C. A. (1978) A new nonpenetrating ballistic injury. *Annals of Surgery*, **188**(6): pp. 753–757.

[14] Wilhelm, M. (2003) A biomechanical assessment of female body armor. Wayne State University Dissertations, 2003.

[15] Wilhelm, M.; Bir, C. (2004) Female body armor assessment: Current methods and future techniques. *Proceedings of Personal Armour Systems Symposium (PASS)*, 2004, Hague, Netherlands.

[16] Gayzik, F. S.; Moreno, D. P.; Vavalle, N. A.; Rhyne, A. C.; Stitzel, J. D. (2012) Development of a full human body finite element model for blunt injury prediction utilizing a multi-modality medical imaging protocol. *12th International LS-DYNA Users Conference*, Detroit.

[17] John, J.; Iraeus, J.; Klug, C.; Svensson, M.; Linder, A. (2020) VIVA+ Open Human Body Models for Virtual Testing. *Automative CAE Grand Challenge (aCAE)*, 2020, online.

[18] Bir, C.; Viano, D.; King, A. (2004) Development of biomechanical response corridors of the thorax to blunt ballistic impacts. *Journal of Biomechanics*, **37**(1): pp. 73–79.

[19] Bir, C.; Viano, D. C. (2004) Design and injury assessment criteria for blunt ballistic impacts. T*he Journal of Trauma*, **57**(6): pp. 1218–1224.

[20] Bass, C. R.; Salzar, R. S., et al. (2006) Injury risk in behind armor blunt thoracic trauma. *International Journal of Occupational Safety and Ergonomics*, **12**(4): pp. 429–442.

[21] Bir, C.; Lance, R.; Stojsih-Sherman, S.; Cavanaugh, J. (2017) Behind Armor Blunt Trauma: Recreation of Field Cases for the Assessment of Back-face Signature Testing. *Proceedings - 30th International Symposium on Ballistics*, 11-15 September 2017, Long Beach, California, USA.

[22] Mertz, H. (1984) A Procedure for Normalizing Impact Response Data. *SAE Government Industry Meeting and Exposition*, May. 21, 1984.

[23] Jenerowicz, M.; Matt, P., et al. (2023) Assessment of GHBMC M50-P Response for Behind Armour Blunt Trauma – Impact Loading with Approximation of 3D Surface of the Armour Back Face Displacement. *Proceedings of IRCOBI Conference*, 2023, Cambridge, UK.

[24] Klein, H.; Jenerowicz, M.; Trube, N.; Boljen, M. (2020) How to Combine 3D Textile Modeling with Latest FE Human Body Models. *Advances in Transdisciplinary Engineering*, **11**: pp. 166–177.

[25] Boljen, M.; Jenerowicz, M.; Bauer, S.; Straßburger, E. (2023) Combining protective clothes with human body models for FE ballistic impact simulations. *CDATP - Communications in Development and Assembling of Textile Products*, Berlin.

[26] B&T. GL06 Granatpistole 40 x 46 mm (2015), https://bt-ag.ch/wp-content/uploads/2020/07/2015_08_gl06_visier.pdf. [09.03.2020].

[27] Clare, V. R.; Lewis, J. H.; Mickiewicz, A. P.; Sturdivan, L. M. (1975) Blunt Trauma Data Correlation. *The Defense Technical Information Center (DTIC), Technical rept.*, Nov. 73–May 74, Maryland, USA.

[28] Sturdivan, L. M.; Viano, D. C.; Champion, H. R. (2004) Analysis of injury criteria to assess chest and abdominal injury risks in blunt and ballistic impacts. *The Journal of Trauma*, **56**(3): pp. 651–663.

[29] Viano, D. C.; Lau, I. V. (1988) A viscous tolerance criterion for soft tissue injury assessment. *Journal of Biomechanics*, **21**(5): pp. 387–399.

[30] Forman, J.; Kulkarni, S.; Perez-Rapela, D.; Mukherjee, S.; Panzer, M.; Hallman, J. (2022) A Method for Thoracic Injury Risk Function Development for Human Body Models. *Proceedings of IRCOBI Conference*, 2022, Porto, Portugal.

[31] Agnew, A. M.; Murach, M. M., et al. (2018) Sources of Variability in Structural Bending Response of Pediatric and Adult Human Ribs in Dynamic Frontal Impacts. *Stapp Car Crash Journal*, **62**: pp. 119–192.